A&A 555, A87 (2013)
DOI: 10.1051/0004-6361/201321714

Astronomy & Astrophysics

Precise radial velocities of giant stars

V. A brown dwarf and a planet orbiting the K giant stars τ Geminorum and 91 Aquarii⋆,⋆⋆

David S. Mitchell[1,2], Sabine Reffert[1], Trifon Trifonov[1], Andreas Quirrenbach[1], and Debra A. Fischer[3]

[1] Landessternwarte, Zentrum für Astronomie der Universität Heidelberg, Königstuhl 12, 69117 Heidelberg, Germany
[2] Physics Department, California Polytechnic State University, San Luis Obispo, CA 93407, USA
e-mail: dsmitche@calpoly.edu
[3] Department of Astronomy, Yale University, New Haven, CT 06511, USA

Received 16 April 2013 / Accepted 22 May 2013

ABSTRACT

Aims. We aim to detect and characterize substellar companions to K giant stars to further our knowledge of planet formation and stellar evolution of intermediate-mass stars.
Methods. For more than a decade we have used Doppler spectroscopy to acquire high-precision radial velocity measurements of K giant stars. All data for this survey were taken at Lick Observatory. Our survey includes 373 G and K giants. Radial velocity data showing periodic variations were fitted with Keplerian orbits using a χ^2 minimization technique.
Results. We report the presence of two substellar companions to the K giant stars τ Gem and 91 Aqr. The brown dwarf orbiting τ Gem has an orbital period of 305.5 ± 0.1 days, a minimum mass of 20.6 M_J, and an eccentricity of 0.031 ± 0.009. The planet orbiting 91 Aqr has an orbital period of 181.4 ± 0.1 days, a minimum mass of 3.2 M_J, and an eccentricity of 0.027 ± 0.026. Both companions have exceptionally circular orbits for their orbital distance, as compared to all previously discovered planetary companions.

Key words. techniques: radial velocities – planets and satellites: detection – brown dwarfs

1. Introduction

Since the discovery of the first extrasolar planets more than 15 years ago, there have been over 700 confirmed extrasolar planet discoveries[1]. Of these planets, more than 60% have been discovered using the radial velocity (RV) technique, though the *Kepler* space telescope has found many more planet candidates that are awaiting confirmation. Thanks to their spectral characteristics, solar-type main sequence stars are the stars most suitable for RV measurements, so they have been the targets of the majority of extrasolar planet searches. However, a growing number of groups are successfully searching for planets around evolved giants and subgiants (e.g. Frink et al. 2002; Sato et al. 2003; Setiawan et al. 2003; Johnson et al. 2006; Lovis & Mayor 2007; Niedzielski et al. 2007; Döllinger et al. 2007).

There are currently 48 known substellar companions orbiting these giant stars, of which 25 have been published during the past four years. These planets allow us to probe more massive stars than are accessible on the main sequence. While main sequence planet searches can typically access stars slightly more massive than our Sun, earlier type stars typically have too few absorption lines for reliable high-precision RV measurements. Evolved stars, such as K giants, have suitable absorption lines for RV measurements, but can have much higher masses. Our sample has typical masses of 1–3 $M_\odot$, and our results show that red giant stars with masses greater than 2.7 $M_\odot$ host very few planets (Reffert et al., in prep.). K giant RV surveys also allow investigating how stellar evolution affects planetary systems.

Our search for planets orbiting giant stars has collected data from 373 stars for over a decade, with several published planet detections (Frink et al. 2002; Reffert et al. 2006; Quirrenbach et al. 2011). In this paper we report substellar companions detected in the RV data of τ Gem (HIP 34693) and 91 Aqr (HIP 114855). These are both single-planet systems at our detection threshold, and both planets have circular orbits. The periodic variations of τ Gem were previously noted in Hekker et al. (2008).

In Sect. 2 we discuss our observations in detail. Section 3 contains information about the stars themselves, including various stellar parameters, and in Sect. 4 we derive the planetary orbits. In Sect. 5 we present evidence against any intrinsic stellar causes of the RV variations. In Sect. 6, we discuss the possible multiplicity of the host stars and the notably low eccentricities of these companions. Finally, in Sect. 7, we summarize our findings.

2. Observations

2.1. Sample selection

Our sample of giant stars started with the selection of 86 K giants brighter than mag 6 in V, showing no signs of duplicity or

⋆ Based on observations collected at Lick Observatory, University of California, and at the European Southern Observatory, Chile, under program IDs 088.D-0132, 089.D-0186, and 090.D-0155.
⋆⋆ Appendices are available in electronic form at http://www.aanda.org
[1] http://www.exoplanets.org

variability. The original selection criteria are described in Frink et al. (2001). Observations of these stars began in June 1999. In June 2000, 96 additional stars were added to the sample with less stringent criteria, such as relaxing the criteria against long-term proper motion and photometric variability. Three stars were removed from the sample when it was discovered that they were visual binaries, leaving a total of 179 stars.

After the detection of several planets orbiting stars in our original sample (Frink et al. 2002; Reffert et al. 2006; Quirrenbach et al. 2011), 194 G and K giants were added to the sample in 2004. These stars were selected for having higher masses and bluer colors on average than the original stars. The higher masses were chosen to test whether or not more massive stars host more massive planetary companions. The color criterion was chosen because bluer stars tend to have less intrinsic jitter than redder stars.

2.2. Radial velocity data

The RV observations were taken at Lick Observatory, using the 0.6 m Coudé Auxiliary Telescope (CAT) with the Hamilton Echelle Spectrograph (Vogt 1987). Our spectra have a resolution of $R \approx 60\,000$, and cover the wavelength range 3755–9590 Å (4725–9590 Å before August 2001). A cell of molecular iodine gas was heated to 50°C and placed in the light path, and the resulting stellar spectra, with iodine absorption lines, were fitted by models created from separate iodine and stellar template spectra. Only the region of the spectrum with iodine absorption lines (5000–5800 Å) is used for this procedure. For dwarf stars, this yields Doppler shifts with precisions better than 3 m s^{-1}. The data acquisition and reduction process is described in more detail in Butler et al. (1996).

We currently have 12–13 years of data for our original set of K giant stars, of which both τ Gem and 91 Aqr are members. We have 95 RV measurements for τ Gem, and 174 for 91 Aqr spaced over this time period. The resulting RV data are given in Tables B.1 and B.2 in Appendix B. Typical exposure times were 15 min for τ Gem and 12 min for 91 Aqr. The signal-to-noise ratios for these observations are typically around 120–150, and the resulting RV measurements have a median precision of 4.7 m s^{-1} for τ Gem and 5.2 m s^{-1} for 91 Aqr. Although this is not the best possible precision available with this method, it is adequate for the requirements of this project. Giant stars typically have larger RV jitter than main sequence stars, on the order of 20 m s^{-1} or larger depending on the individual star (Hekker et al. 2006), so improved precision would not be beneficial to the detection of a planetary RV signal.

3. Stellar properties

The stellar properties of both stars are given in Table 1. Visual magnitude and parallax measurements are taken from Hipparcos observations (van Leeuwen 2007). K magnitude values are taken from 2MASS (Skrutskie et al. 2006). Hekker & Meléndez (2007) measured the metallicity of these stars, using our spectra for their analysis. While τ Gem is slightly metal-rich, 91 Aqr has about solar metallicity.

In order to derive stellar parameters such as mass, surface gravity, effective temperature, stellar radius and stellar age, the evolutionary tracks of Girardi et al. (2000) were interpolated onto the observed $B - V$ color, absolute V magnitude (van Leeuwen 2007), and metallicity (Hekker & Meléndez 2007; trilinear interpolation). In general, this approach resulted in two possible solutions, depending on the precise evolutionary status (red giant branch or horizontal branch) of the star. Probabilities were assigned to each solution, taking the evolutionary timescale (the speed with which the star moves through that portion of the evolutionary track) as well as the initial mass functions into account (Künstler 2008). More details on the method as well as the stellar parameters for all K giant stars on our Doppler program can be found in Reffert et al. (in prep.).

Table 1. Stellar parameters.

Parameter	τ Gem HIP 34693	91 Aqr HIP 114855
Spectral type	K2III	K0III
m_v [mag][a]	4.41	4.24
M_v [mag]	-0.56 ± 0.05	0.93 ± 0.03
K [mag][b]	1.681 ± 0.254	1.597 ± 0.236
$B - V$ [mag][a]	1.261 ± 0.000	1.107 ± 0.005
Parallax [mas][a]	10.16 ± 0.25	21.78 ± 0.29
Distance [pc]	$98.4 \pm {}^{2.5}_{2.4}$	45.9 ± 0.6
Radius [$R_\odot$][c]	26.8 ± 0.7	11.0 ± 0.1
$T_{\rm eff}$ [K][c]	4388 ± 25	4665 ± 18
$\log g$ [cm s^{-2}][c]	1.96 ± 0.08	2.52 ± 0.05
[Fe/H][d]	0.14 ± 0.1	-0.03 ± 0.1
Mass [$M_\odot$][c]	2.3 ± 0.3	1.4 ± 0.1
Age [Gyr][c]	1.22 ± 0.76	3.56 ± 0.63
Absolute RV [km s^{-1}][e]	22	-26
$v \sin i$ [km s^{-1}]	<1.0[f]	3.9 ± 0.5[g]

References. [(a)] Data from Hipparcos: van Leeuwen (2007). [(b)] Data from 2MASS: Skrutskie et al. (2006). [(c)] Künstler (2008). [(d)] Hekker & Meléndez (2007). [(e)] This paper, data acquired using CRIRES, see Sect. 5.2. [(f)] de Medeiros & Mayor (1999). [(g)] Tokovinin & Smekhov (2002).

Both of these stars were determined to be more likely on the HB by this method. τ Gem was found to have a 64% chance of being on the HB, and 91 Aqr has a 79% chance of being on the HB. If the stars are RGB stars, the masses would be $2.5 \pm 0.3\ M_\odot$ for τ Gem and $1.6 \pm 0.2\ M_\odot$ for 91 Aqr.

Absolute RV measurements were taken using the CRIRES spectrograph (Käufl et al. 2004). The $v \sin i$ limit for τ Gem was measured by de Medeiros & Mayor (1999), while the value for 91 Aqr was measured by Tokovinin & Smekhov (2002).

4. Keplerian orbit

The RV data of τ Gem and 91 Aqr are shown in Figs. 1 and 2, along with the best Keplerian fit to the data (upper panels). The lower panels show the residual RV data, after subtraction of the Keplerian fits. Error bars are included in all plots, but in many cases are too small to be visible.

For each orbital solution there were six parameters fit to the data: five orbital parameters and the zero-level of the RV data, which was not constrained by our measurements. The five orbital parameters are the orbital period (P), the periastron time (T_0), the longitude of periastron (ω), the orbital eccentricity (e), and the semi-major axis of the stellar orbit ($a_1 \sin i$). All of the fitted parameters, with the exception of the RV zero-point, are included in Table 2. Uncertainties shown in those tables are based on the χ^2 fit. We found no signature of stellar astrometric motion due to these companions in the Hipparcos data, and because the threshold for detecting this motion with Hipparcos is rather high, no meaningful constraints could be placed on either the companion mass or orbital inclination for either planet.

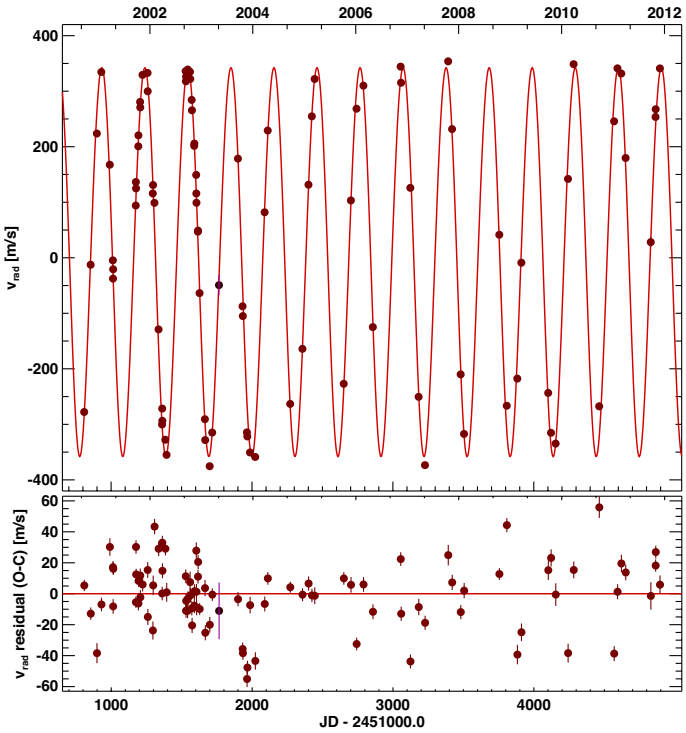

Fig. 1. Radial velocity plot for τ Gem. *Top panel*: RV data with best Keplerian fit. *Bottom panel*: residual RV data after subtraction of best fit.

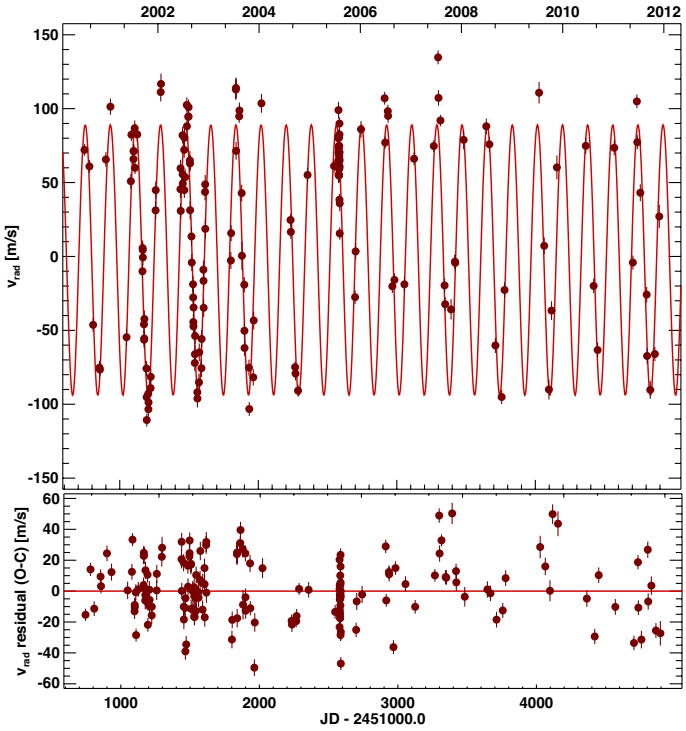

Fig. 2. Radial velocity plot for 91 Aqr. *Top panel*: RV data with best Keplerian fit. *Bottom panel*: residual RV data after subtraction of best fit.

Fitting orbits with these standard orbital parameters can cause problems when the orbits have low eccentricities. For example, the periastron time has very large errors by definition, if the eccentricity is low. For this reason we also fitted the data using the following five orbital parameters: $\log P$, $\log K_1$ (where K_1 is the semi-amplitude of the RV), $e\cos(\omega)$, $e\sin(\omega)$, and λ_0 (where λ_0 is the sum of the longitude of the periastron and the mean anomaly). Fitting the data with these parameters resulted in no significant difference to the orbital solution or the uncertainties. We also used the revised Lucy-Sweeney test (Lucy 2013) to see whether an upper limit to the eccentricities would be more appropriate. While the derived eccentricity of τ Gem was a sufficient number of standard deviations away from zero to be accurate, this method suggests that the eccentricity of 91 Aqr is more appropriately described as less than 0.034 at the one sigma confidence level, and for the 95% confidence level, less than 0.064.

Periodograms for our data are shown in Figs. 3 and 4. The top panels show the results for the RV data. Each star has a single, strong peak at a period matching the Keplerian fit to the data. The periodogram for 91 Aqr has several additional peaks that are weaker but significant. All of these peaks are due to aliasing effects. The two large peaks on either side of the physical peak are yearly aliases. To the left of the main peak is a peak corresponding to the physical frequency f_0 added to the annual frequency $f_{\rm year}$. To the right is a double peak which combines both $f_0 - f_{\rm year}$ and $f_{\rm year}$ alone. These two peaks overlap because the orbital period of this companion is very close to half a year. At shorter periods there are smaller peaks at one month and at 14 and 16 days. These are due to our observing schedule. We were usually scheduled for either bi-monthly observing runs or dark time observing runs every month, thus these aliases represent our observation frequencies. All of the aliases seen here are typical for RV planet searches (Dawson & Fabrycky 2010).

Table 2. Best fit orbital parameters.

Parameter	τ Gem	91 Aqr
P [days]	305.5 ± 0.1	181.4 ± 0.1
T_0 [JD-2 450 000]	3270.7 ± 14.8	3472.1 ± 24.5
e	0.031 ± 0.009	0.027 ± 0.026
ω [°]	137.4 ± 0.3	177.3 ± 0.8
$a_1 \sin(i)$ [10^{-3}AU]	9.83 ± 0.09	1.53 ± 0.04
$f(m)$ [$10^{-8} M_\odot$]	136	1.44
a_2 [AU]	1.17	0.70
K_1 [m s^{-1}]	350.2	91.5
$m_2 \sin(i)$ [M_J]	20.6	3.2
Reduced χ^2	19.8	14.0
rms scatter around fit [m s^{-1}]	21.9	18.9

The bottom panels of Figs. 3 and 4 show a periodogram of the data after the Keplerian fit has been removed. Neither star has any significant periodicity in the residuals. The residual radial velocities, after subtraction of the best Keplerian fits, are consistent with the small intrinsic scatter expected from K-giant stars, at a level of around 20 m s^{-1} (Frink et al. 2001).

5. Intrinsic stellar effects

In addition to planetary or stellar companions, intrinsic stellar activity can also cause RV variations in giant stars. This makes detections of substellar companions around K giants somewhat more challenging than around inactive stars, since one has to demonstrate that the interpretation of the observed RV pattern is due to the companion and not due to intrinsic effects. This has been discussed in detail by Hatzes et al. (2004).

Features on the surface of a star, such as hot or cool spots or plages, can create asymmetries in the stellar absorption lines (Walker et al. 1992). This asymmetry is seen as a shift in the RV of the star, and as the star rotates, the Doppler shift will vary periodically.

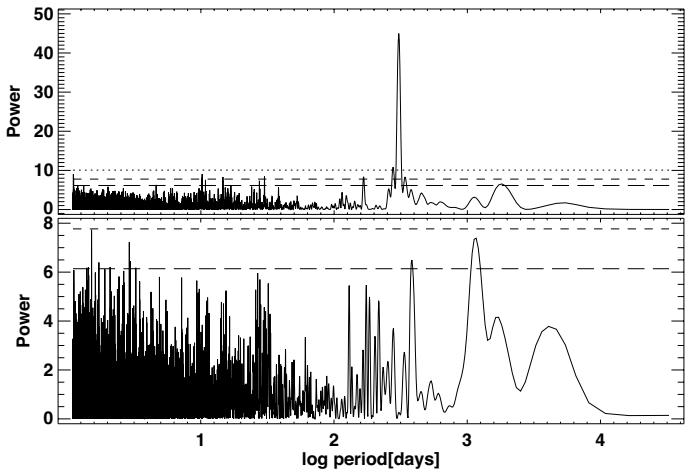

Fig. 3. *Top*: periodogram of the RV data for τ Gem. There is a significant peak at 305.5 days, matching the best Keplerian orbital fit. The dotted/hyphen/dashed lines show false alarm probabilities of 0.001, 0.01, and 0.05 respectively. *Bottom*: periodogram for the residual data after subtraction of the orbital fit. There is no significant peak present.

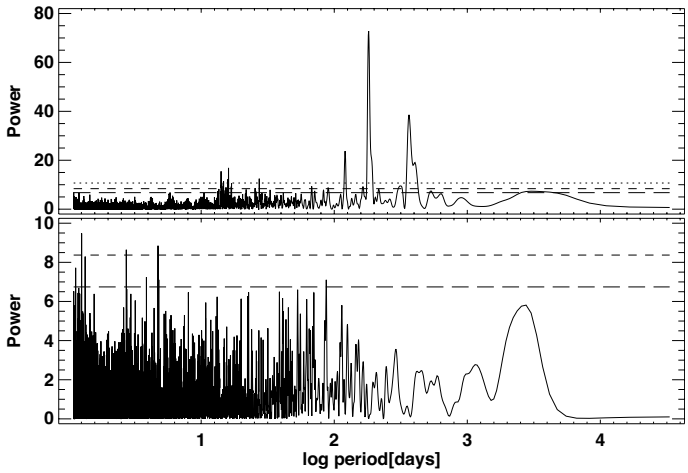

Fig. 4. *Top*: periodogram of the RV data for 91 Aqr. There is a significant peak at 181.4 days, matching the best Keplerian orbital fit. The dotted/hyphen/dashed lines show false alarm probabilities of 0.001, 0.01, and 0.05 respectively. *Bottom*: periodogram for the residual data after subtraction of the orbital fit. There is no significant peak present.

The radius of taugem is 26.8 $R_\odot$ and the $v \sin i$ is less than 1 km s^{-1}. If one assumes that rotational effects are causing the RV variations, then the rotation period of the star must be the same as the period of the RV data, 306 days, leading to a rotational velocity of 4.4 km s^{-1}. This puts an upper limit on the inclination angle of the star at 13°.0. With this limit in place, if one assumes starspots 800 K cooler than the stellar surface temperature, the starspots would need to be larger than 50% of the surface of the star, and there would be photometric signatures of such a feature many times larger than the HIPPARCOS limit of 0.02 magnitudes. Therefore rotational modulation cannot be the source of RV variability in τ Gem.

The radius of 91 Aqr is 11.0 $R_\odot$ and the RV period is 181 days. This would imply a rotational velocity of 3.0 km s^{-1}, which is less than the observed rotational velocity of 3.9 km s^{-1}. Given that the uncertainty for the implied rotational velocity is less than 0.1 km s^{-1}and the uncertainty on the measured rotational velocity is 0.5 km s^{-1}, rotational modulation is not a viable explanation for the 181 day period we observe in 91 Aqr.

Some K giants are known to be pulsating stars. Not all of them pulsate, and those that do typically display several modes at different frequencies, and with different amplitudes (Hatzes & Cochran 1993). The pulsations of a star cause parts of the surface of the star to move toward the observer, and other parts of the surface to move away from the observer, such that the RV measurements will be affected. Thus, a particular pulsation frequency in a star may cause RV variations with the same frequency.

Pulsations can be characterized as radial and non-radial. Radial pulsations are the simplest pulsation, where the entire star grows and shrinks with a single frequency. K giant stars typically have radial pulsation periods of a few days. Using the method of Cox et al. (1972), we estimate that the radial pulsation periods of 91 Aqr should be about 2.6 days, and that of τ Gem about 3.0 days. It is clear that the radial pulsation periods for these stars are several orders of magnitude smaller than the RV periods, ruling out radial pulsations as the possible cause.

Non-radial pulsations are much more complicated to identify than radial pulsations. Any number of periods and amplitudes are possible for the various modes. However one would not expect the RV amplitude of the pulsations in the visible waveband to match the amplitude in the infrared, since the photometric variations of pulsating stars are different at visible and infrared wavelengths (Percy et al. 2001). On the other hand, if the RV variations are due to a companion, the IR and visible RV variations should be identical. Comparing RV amplitudes at different wavelengths has also proven useful in detecting intrinsic stellar variations, even in cases where measuring line bisector variations failed to do so (Prato et al. 2008).

During 2012 and 2013 we observed both of our stars with the high-resolution IR spectrograph CRIRES (Käufl et al. 2004) at the Very Large Telescope (VLT). CRIRES spectra have a resolution of $R \approx 100\,000$ when used with the 0.2" slit. Our spectra cover the wavelength range 1.57–1.61 μm, characterized by many deep and sharp telluric lines used as references. To determine RV measurements from these data, we followed a procedure similar to that of Figueira et al. (2010). First we reduced the data using the standard ESO CRIRES reduction pipeline. Then we obtained precise R measurements by cross-correlating a synthetic spectrum with the CRIRES spectra. Our RV measurements using CRIRES have an estimated uncertainty of 40 m s^{-1}. The CRIRES data for both stars are given in Tables B.3 and B.4 in Appendix B. After collecting the RV measurements from CRIRES, a best fit offset value was calculated for each of the stars, to fit the IR data to the previously calculated orbital fit to the visible RV data.

Figures 5 and 6 show the CRIRES data. The top panels of the figures show the CRIRES data plotted against the Keplerian fit to the Lick data. The bottoms of the figures show the residuals of the CRIRES data after subtraction of the fit. The scatter around the fit is consistent with intrinsic jitter of the star. These plots show that the RV variations in these stars have the same amplitude and phase in both visible and IR bandpasses, confirming that the source of the variations are the companions and not intrinsic variations.

6. Discussion

6.1. Stellar multiplicity

Both of the stars discussed in this paper are listed in the literature as being multiple stars. τ Gem is indicated in the Washington Double Star catalog (WDS; Mason et al. 2001) as having two

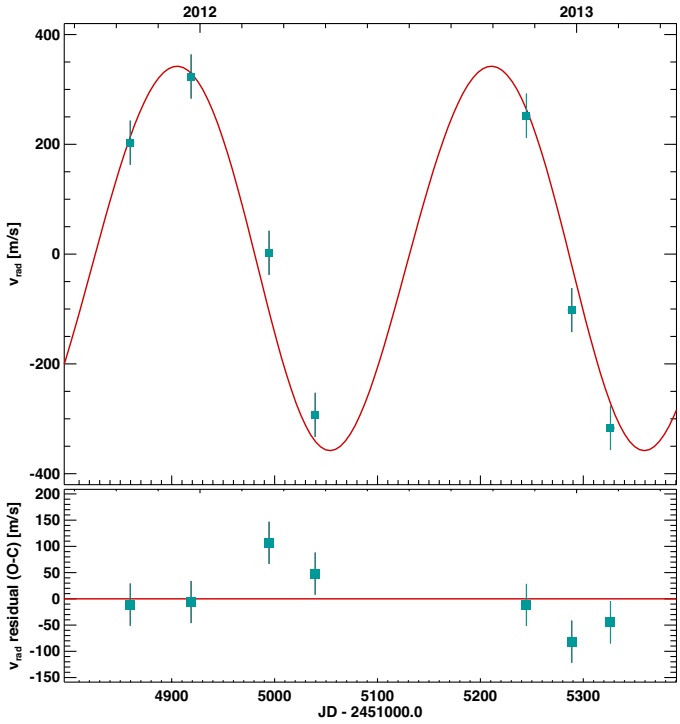

Fig. 5. *Top panel*: τ Gem CRIRES infrared RV data with orbital fit from Lick data. *Bottom panel*: residual CRIRES data after subtraction of fit.

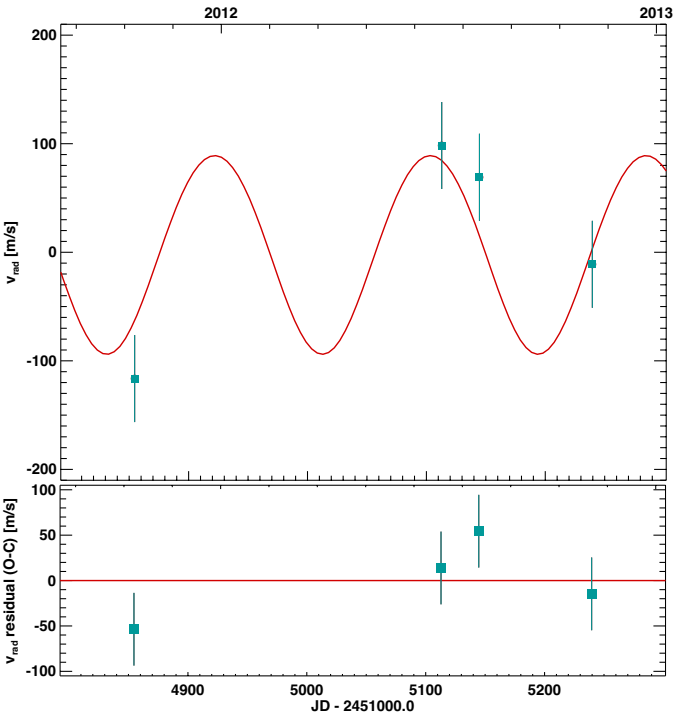

Fig. 6. *Top panel*: 91 Aqr CRIRES infrared RV data with orbital fit from Lick data. *Bottom panel*: residual CRIRES data after subtraction of fit.

companion stars. The primary companion was measured to be separated by 2″, and has a visual magnitude of m_v = 11.0 mag. More recent observation by HIPPARCOS did not detect this secondary component. This component is most likely physically connected to our star, based on the very small separation. At the HIPPARCOS distance of 98.4 pc, the secondary star would be a K0 dwarf, separated by about 187 AU.

For a star with a companion of known mass and separation, one can find the maximum rate of change for the radial velocity of any orbit to be

$$a_{z_{\max}} = \frac{2Gm_c\varpi^2}{3\sqrt{3}\rho^2} \quad (1)$$

where G is the gravitational constant, m_c is the companion mass, ϖ is the parallax for the stars and ρ is the angular separation between the stars. The derivation of this equation is given in Appendix A. If we assume that the companion here is a K0 dwarf of mass 0.8 $M_\odot$, then the maximum RV change would be 1.6 m/s/yr, which could be detectable with our current data. However, many orbits with RV variations below our detection threshold are also possible.

An additional companion is listed in the WDS, at a separation of about 59″, and a magnitude of m_v = 12.4 mag, though the physical connection of this component is dubious. This would correspond to a physical separation of well over 5000 AU, which would not be visible in our RV data.

WDS lists 91 Aqr as a member of a quintuple star system. The primary companion to 91 Aqr is a visual binary pair of magnitudes 10.5 and 10.7, separated from the primary component by 50″. At the HIPPARCOS distance of 45.9 pc, this would lead to a separation of over 2000 AU, too large to be visible in the RV data. Raghavan et al. (2006) show that the primary companion to 91 Aqr is a binary star pair by matching the proper motion and radial velocities of the two components, and by comparing spectroscopic parallaxes.

Zirm (2007) derived the orbit of the BC components as having an orbital period of 83.6 yr, a semi-major axis of 0.″47, an eccentricity of 0.45, and an inclination of 87°, which is nearly edge-on. This semi-major axis corresponds to 21.5 AU.

Raghavan et al. (2006) also show that the other two companions listed in the WDS are in fact field stars. Thus, 91 Aqr b is one of a handful of planets in a triple star system.

6.2. Brown dwarf companions

It is well established that Sun-like main sequence stars are much more likely to have planetary mass companions than brown dwarf companions (Marcy & Butler 2000). From the California & Carnegie Planet Search and the McDonald Observatory Planet Search, the frequency at which we find brown dwarf companions orbiting Sun-like main sequence stars with orbital periods less than five years is less than 1% (e.g. Vogt et al. 2002; Patel et al. 2007; Wittenmyer et al. 2009). By controlling for selection effects, Grether & Lineweaver (2006) approximate the fraction of Sun-like stars harboring giant planet companions with orbits less than 5 years to be 5 ± 2%, and the fraction of such stars harboring brown dwarf companions at close orbits to be less than 1%. Since they also calculated that 11 ± 3% of Sun-like stars have stellar companions at close orbits, this demonstrates the relative paucity of companions in the brown dwarf mass regime, compared to both higher and lower masses.

It appears that giant stars may host more brown dwarfs than solar-type main sequence stars. To date, 10 companions in the brown dwarf mass regime have been found around giant stars, as compared to nine brown dwarfs orbiting main sequence stars and two orbiting subgiants. Three of the nine main sequence companions were discovered with transit observations. This is all true despite the giant stars being more massive, on average, than the stars in the main sequence samples, making RV detections more difficult due to the smaller amplitudes, and despite the

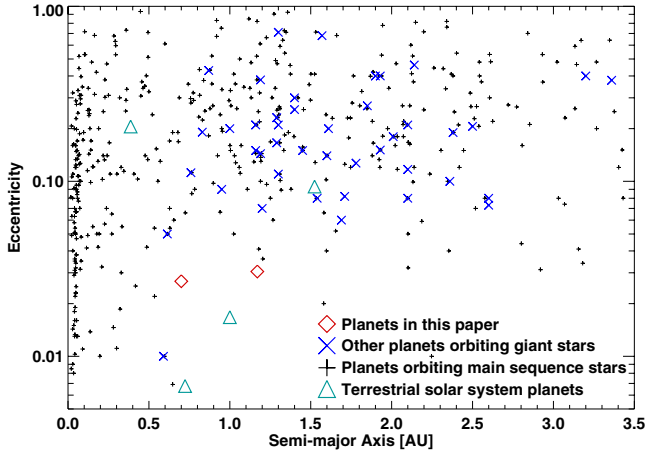

Fig. 7. Eccentricities for substellar companions. Companions from this paper are shown as diamonds, all other companions of giant stars are shown with a cross. Companions to main sequence stars are shown as small plusses. Terrestrial planets from our solar system are shown as triangles.

giant star surveys having a smaller stellar sample. It is difficult to estimate the rate of brown dwarf detection in giant stars, due to the less complete nature of these surveys, and the large and varying amount of stellar jitter in these stars. However, it seems likely that brown dwarfs are not quite so rare around the more massive, evolved stars of the giant surveys, as these more massive stars would have had more massive protoplanetary disks from which to form companions.

6.3. Eccentricity

Both of the planetary orbits described here are extremely circular. In fact, they could be considered the most circular orbits found among planets orbiting at this distance from their host star. Figure 7 shows the orbital eccentricity of known extrasolar planets plotted against the semi-major axis of their orbits. Symbols for the different categories of planets are given in the plot. Planets with orbits greater than 3.5 AU are omitted, as are planets without properly measured values and uncertainties for the orbital eccentricity. Orbital values for the companions to Pollux and ν Oph are taken from our data, since it is the most extensive RV data set for these stars, with the best available orbital fits. There are, however, other published values (Hatzes et al. 2006; Sato et al. 2012). In particular, the alternate published value for the companion to Pollux lists an eccentricity of 0.02 ± 0.03, as opposed to our current best fit value of 0.05 ± 0.01.

From the plot it is clear that one must look at closer orbits to find planets with as circular orbits as the planets described here, with a few possible exceptions. One other K giant companion has a lower published eccentricity, (HD 32518 b, Döllinger et al. 2009), but the value for that eccentricity is questionable. The published value for HD 32518 b is $e = 0.01 \pm 0.03$, which according to the Lucy-Sweeney test should be replaced by an upper limit on the eccentricity of 0.06 for the 95% confidence level, and at the one sigma level the upper limit would be 0.03. This is approximately the same value as the two orbits presented in this paper, but with larger uncertainty.

A more interesting planet with a more circular orbit than those presented here has an eccentricity of $0.0069 \pm {}^{0.0010}_{0.0015}$ and semi-major axis of 0.65 AU (Doyle et al. 2011). This is the famous circumbinary planet Kepler 16 b. A second interesting planet with a similar orbit (though larger semi-major axis) is HD 60532 c (Desort et al. 2008). This is the outer of two planets orbiting this star, orbiting at 1.58 AU with an eccentricity of 0.02 ± 0.02. Again, using the Lucy-Sweeney test, this might more accurately be considered an orbit with an upper limit to the eccentricity of 0.05 for the 95% confidence level, and 0.03 for the one sigma confidence level. It is also interesting to note that the authors of this discovery believe there to be significant interaction between these two planets, including a possible 3-to-1 orbital resonance, with variations in the semi-major axis and eccentricity of the orbits.

Finally, one last notable planet is one with a semi-major axis of 2.25 AU, and an eccentricity of 0.01 ± 0.03: HD 159868 c (Wittenmyer et al. 2012). Like HD 60532 c, this is the outer planet of a two-planet system where interactions are possible, though the orbits are stable. Like HD 32518 b, the uncertainty on the eccentricity is so high that an upper limit of 0.03 (for one sigma confidence) is appropriate.

Several groups have investigated the theoretical effects of stellar evolution on the orbits of planets (Villaver & Livio 2009; Kunitomo et al. 2011). Though these studies have focused on the change in semi-major axis of the planet, and the possibility of engulfment by the RGB star, presumably planets just outside the engulfment limit will still be strongly affected by the star's tidal forces. Effects of this interaction might include orbital circularization. Another possibility is that planets beyond a critical distance may evolve into orbits with a larger semi-major axis due to mass loss by the host star. Even though one is far more likely to find circular orbits for closely orbiting planets, either of these phenomena could explain more distant orbits, such as those described here, having very low eccentricities. It is interesting that the only planets discovered with similar orbits to the planets discussed in this paper are in multiple planetary systems that likely interact, orbit a binary star, or are orbiting evolved stars.

7. Summary

In this paper we report the detection of two substellar companions orbiting the K giant stars τ Gem and 91 Aqr, using the Hamilton spectrograph at Lick Observatory. The companion to τ Gem has a minimum mass of 20.6 M_J, putting it in the brown dwarf regime. The companion to 91 Aqr has a minimum mass of 3.2 M_J, putting it in the giant planet mass range. Both companions have extremely circular orbits, especially considering their relatively distant orbits, and the orbital characteristics have been stable over more than 12 years of observation. RV data taken in the IR match the orbital fit, confirming the presence of a companion as the source of the RV variations.

Acknowledgements. We would like to thank the staff at Lick Observatory for their support over the years of this project. We would like to thank the CAT observers that assisted with this project, including Saskia Hekker, Christian Schwab, Simon Albrecht, David Bauer, Christoph Bergmann, Stanley Browne, Kelsey Clubb, Dennis Kügler, Julian Stürmer, Kirsten Vincke, and Dominika Wylezalek. We graciously acknowledge the work of Geoffrey Marcy in creating the iodine cell system at Lick Observatory, and writing the original Doppler code. We thank Mathias Zechmeister and Ansgar Reiners for their help with the acquisition and reduction of the CRIRES data. This research has made use of the SIMBAD database and the VizieR catalog access tool, CDS, Strasbourg, France. This publication makes use of data products from the Two Micron All Sky Survey, which is a joint project of the University of Massachusetts and the Infrared Processing and Analysis Center/California Institute of Technology, funded by the National Aeronautics and Space Administration and the National Science Foundation. This research has made use of the Washington Double Star Catalog maintained at the US Naval Observatory. This research has made use of the Exoplanet Orbit Database and the Exoplanet Data Explorer at exoplanets.org.

References

Butler, R. P., Marcy, G. W., Williams, E., et al. 1996, PASP, 108, 500
Cox, J. P., King, D. S., & Stellingwerf, R. F. 1972, ApJ, 171, 93
Dawson, R. I., & Fabrycky, D. C. 2010, ApJ, 722, 937
de Medeiros, J. R., & Mayor, M. 1999, A&AS, 139, 433
Desort, M., Lagrange, A.-M., Galland, F., et al. 2008, A&A, 491, 883
Döllinger, M. P., Hatzes, A. P., Pasquini, L., et al. 2007, A&A, 472, 649
Döllinger, M. P., Hatzes, A. P., Pasquini, L., Guenther, E. W., & Hartmann, M. 2009, A&A, 505, 1311
Doyle, L. R., Carter, J. A., Fabrycky, D. C., et al. 2011, Science, 333, 1602
Figueira, P., Pepe, F., Melo, C. H. F., et al. 2010, A&A, 511, A55
Frink, S., Quirrenbach, A., Fischer, D., Röser, S., & Schilbach, E. 2001, PASP, 113, 173
Frink, S., Mitchell, D. S., Quirrenbach, A., et al. 2002, ApJ, 576, 478
Girardi, L., Bressan, A., Bertelli, G., & Chiosi, C. 2000, A&AS, 141, 371
Grether, D., & Lineweaver, C. H. 2006, ApJ, 640, 1051
Hatzes, A. P. & Cochran, W. D. 1993, ApJ, 413, 339
Hatzes, A. P., Setiawan, J., Pasquini, L., & da Silva, L. 2004, in Stellar Structure and Habitable Planet Finding, eds. F. Favata, S. Aigrain, & A. Wilson, ESA Spec. Publ., 538, 87
Hatzes, A. P., Cochran, W. D., Endl, M., et al. 2006, A&A, 457, 335
Hekker, S., & Meléndez, J. 2007, A&A, 475, 1003
Hekker, S., Reffert, S., Quirrenbach, A., et al. 2006, A&A, 454, 943
Hekker, S., Snellen, I. A. G., Aerts, C., et al. 2008, A&A, 480, 215
Johnson, J. A., Marcy, G. W., Fischer, D. A., et al. 2006, ApJ, 652, 1724
Käufl, H.-U., Ballester, P., Biereichel, P., et al. 2004, in SPIE Conf. Ser. 5492, eds. A. F. M. Moorwood & M. Iye, 1218
Kunitomo, M., Ikoma, M., Sato, B., Katsuta, Y., & Ida, S. 2011, ApJ, 737, 66
Künstler, A. 2008, Diplomarbeit, Landessternwarte, Heidelberg University, Germany
Lovis, C., & Mayor, M. 2007, A&A, 472, 657
Lucy, L. B. 2013, A&A, 551, A47
Marcy, G. W., & Butler, R. P. 2000, PASP, 112, 137
Mason, B. D., Wycoff, G. L., Hartkopf, W. I., Douglass, G. G., & Worley, C. E. 2001, AJ, 122, 3466
Niedzielski, A., Konacki, M., Wolszczan, A., et al. 2007, ApJ, 669, 1354
Patel, S. G., Vogt, S. S., Marcy, G. W., et al. 2007, ApJ, 665, 744
Percy, J. R., Wilson, J. B., & Henry, G. W. 2001, PASP, 113, 983
Prato, L., Huerta, M., Johns-Krull, C. M., et al. 2008, ApJ, 687, L103
Quirrenbach, A., Reffert, S., & Bergmann, C. 2011, in AIP Conf. Ser. 1331, eds. S. Schuh, H. Drechsel, & U. Heber, 102
Raghavan, D., Henry, T. J., Mason, B. D., et al. 2006, ApJ, 646, 523
Reffert, S., Quirrenbach, A., Mitchell, D. S., et al. 2006, ApJ, 652, 661
Sato, B., Ando, H., Kambe, E., et al. 2003, ApJ, 597, L157
Sato, B., Omiya, M., Harakawa, H., et al. 2012, PASJ, 64, 135
Setiawan, J., Hatzes, A. P., von der Lühe, O., et al. 2003, A&A, 398, L19
Skrutskie, M. F., Cutri, R. M., Stiening, R., et al. 2006, AJ, 131, 1163
Tokovinin, A. A., & Smekhov, M. G. 2002, A&A, 382, 118
van Leeuwen, F. 2007, A&A, 474, 653
Villaver, E., & Livio, M. 2009, ApJ, 705, L81
Vogt, S. S. 1987, PASP, 99, 1214
Vogt, S. S., Butler, R. P., Marcy, G. W., et al. 2002, ApJ, 568, 352
Walker, G. A. H., Bohlender, D. A., Walker, A. R., et al. 1992, ApJ, 396, L91
Wittenmyer, R. A., Endl, M., Cochran, W. D., et al. 2009, AJ, 137, 3529
Wittenmyer, R. A., Horner, J., Tuomi, M., et al. 2012, ApJ, 753, 169
Zirm, H. 2007, IAU Commission on Double Stars, 161, 1

Pages 8 to 10 are available in the electronic edition of the journal at http://www.aanda.org

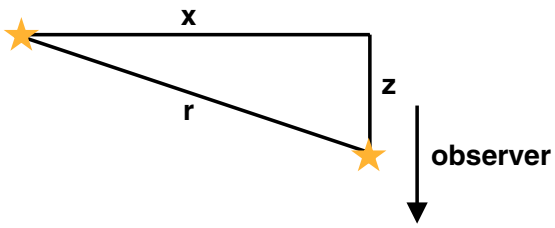

Fig. A.1. Diagram of binary star system. The star of interest is on the right and the companion is on the left. The observer is below the system in the plane of the page, so that the separation r can be broken into the component along the line of sight, z, and the projection of the separation visible to the observer, x.

Appendix A: Maximum RV change for stars with companions

In the case of a visual binary star system, one might not have any information about the orbit other than the current separation. In this case, one can still calculate the maximum RV change of any orbit in that configuration, as long as the distance to the system is known.

Figure A.1 shows the orientation of our system. The star and companion are separated by distance r. If we assume the observer is in the plane of the page, then we can break that distance into the x component, the projection of the separation visible to the observer, and the z component along the line of sight. We know that the acceleration of our star of interest, due to the gravitational interaction with its companion, is

$$a = \frac{Gm_c}{r^2} \tag{A.1}$$

where G is the gravitational constant, m_c is the companion mass, and r is the physical separation between them. Since we do not know the physical separation, but instead only have the projection of this separation, we must find the acceleration in terms of the projected separation x and the component of the separation along our line of sight, z. Here we are only concerned with the acceleration along our line of sight, which is

$$a_z = \frac{Gm_c z}{(x^2 + z^2)^{\frac{3}{2}}}. \tag{A.2}$$

To find the maximum value for the acceleration we must differentiate,

$$\frac{\mathrm{d}a_z}{\mathrm{d}z} = \frac{Gm_c\left(x^2 - 2z^2\right)}{(x^2 + z^2)^{\frac{5}{2}}}, \tag{A.3}$$

then set this equal to zero. This gives

$$z_{\max} = \frac{x}{\sqrt{2}} \tag{A.4}$$

which is the condition at the maximum acceleration. Inserting this back into Eq. (A.2), and putting the projected separation x in terms of the observed angular separation ρ and the parallax ϖ, gives the maximum acceleration along the line of site

$$a_{z_{\max}} = \frac{2Gm_c\varpi^2}{3\sqrt{3}\rho^2} \tag{A.5}$$

for any orbit of a star with a companion of given mass.

Appendix B: RV data

Table B.1. RV data for τ Gem.

JD[a] [days]	$v_{\rm rad}$ [m s^{-1}]	$\sigma_{\rm RV}$ [m s^{-1}]
1809.039	−277.8	3.6
1854.888	−12.6	4.0
1898.902	223.8	6.5
1930.810	334.5	4.4
1990.659	167.6	5.6
2012.653	−4.7	4.0
2013.651	−37.5	4.7
2014.656	−20.8	4.0
2175.047	94.1	3.7
2176.055	136.4	4.3
2177.035	124.9	3.6
2192.995	200.7	4.5
2193.967	220.5	3.8
2205.938	280.7	4.5
2206.949	270.7	4.6
2222.898	329.3	4.5
2258.811	332.9	5.1
2259.853	299.8	5.1
2295.773	115.8	5.8
2297.842	131.0	6.3
2307.730	98.9	5.0
2336.741	−129.0	4.8
2361.708	−300.2	4.4
2362.721	−271.6	4.5
2363.688	−293.6	4.8
2384.667	−327.7	4.3
2393.654	−354.9	6.1
2529.039	336.2	4.4
2531.009	317.8	4.6
2532.039	326.1	4.3
2542.018	330.5	4.7
2543.981	339.0	4.7
2560.013	334.8	6.8
2562.004	322.0	4.6
2571.969	284.3	4.6
2574.010	265.6	4.9
2589.975	201.6	4.8
2590.892	205.7	4.5
2603.925	149.2	5.3
2604.916	115.8	5.1
2605.867	99.1	5.1
2615.842	47.0	4.5
2616.858	48.9	4.5
2627.816	−63.7	3.8
2665.755	−290.7	5.2
2667.815	−328.3	4.9
2699.687	−375.4	5.1
2717.691	−314.8	4.1
2765.676	−49.3	18.3
2900.034	178.6	4.6
2932.987	−87.4	4.2
2934.975	−105.0	4.3
2964.028	−314.4	5.2
2966.896	−321.8	4.3
2985.944	−350.6	5.3
3022.849	−358.7	5.6
3089.704	81.9	4.8
3111.665	229.1	4.1
3271.015	−263.2	3.6
3357.929	−164.1	4.2
3400.811	131.6	4.6
3424.711	254.7	4.3
3444.674	322.0	5.5

Notes. [(a)] Julian date – 2 450 000.

Table B.1. continued.

JD[a] [days]	v_{rad} [m s^{-1}]	σ_{RV} [m s^{-1}]
3651.003	−227.0	4.1
3701.974	103.2	5.1
3741.888	268.5	4.1
3790.746	310.0	4.7
3857.654	−124.8	4.8
4054.935	344.2	4.4
4057.940	315.3	4.6
4123.835	126.0	4.5
4182.662	−250.5	5.3
4227.649	−373.4	4.6
4392.004	353.7	6.6
4419.958	231.7	4.9
4480.917	−210.0	4.6
4504.767	−317.3	4.9
4754.975	41.5	3.8
4807.924	−266.5	4.6
4882.830	−217.6	6.3
4911.674	−8.9	5.7
5102.055	−243.4	6.4
5122.025	−315.3	5.5
5154.966	−334.6	7.3
5242.708	142.0	6.1
5282.681	348.6	5.4
5464.063	−267.5	6.9
5569.854	245.8	4.8
5593.771	341.2	4.9
5620.740	331.8	5.7
5651.688	179.7	5.1
5830.017	28.2	8.9
5863.951	253.6	4.0
5865.031	267.5	4.1
5894.944	341.1	6.1

Table B.2. RV data for 91 Aqr.

JD[a] [days]	v_{rad} [m s^{-1}]	σ_{RV} [m s^{-1}]
1744.976	72.1	3.9
1780.886	60.9	4.3
1807.843	−46.3	4.8
1853.694	−75.3	4.7
1856.737	−76.5	4.6
1899.645	65.6	5.0
1932.598	101.3	5.5
2049.000	−54.6	5.7
2079.999	50.9	5.1
2083.991	82.4	4.2
2098.992	65.9	5.0
2099.962	71.3	4.7
2100.982	71.2	4.7
2107.959	86.8	5.2
2109.955	60.0	4.2
2125.939	82.6	4.7
2163.837	−10.0	4.9
2164.896	5.7	5.1
2165.868	4.5	4.6
2166.885	−0.7	5.4
2174.843	−45.9	5.2
2175.820	−56.4	5.8
2176.798	−55.5	4.7
2177.826	−42.3	5.7
2192.772	−75.8	5.0
2193.805	−95.2	5.0
2194.786	−110.7	4.4

Notes. [(a)] Julian date – 2 450 000.

Table B.2. continued.

JD[a] [days]	v_{rad} [m s^{-1}]	σ_{RV} [m s^{-1}]
2205.714	−92.8	5.6
2206.754	−103.4	5.1
2207.716	−98.8	5.3
2222.754	−89.1	5.7
2223.698	−81.4	5.5
2258.635	31.2	6.2
2259.675	44.9	5.8
2295.594	111.2	6.3
2297.595	116.8	7.0
2437.985	45.5	6.0
2438.963	59.6	5.7
2439.990	30.8	5.2
2452.995	82.0	5.5
2453.944	55.5	5.6
2454.958	49.3	6.2
2464.987	72.1	5.3
2465.954	44.9	5.4
2466.975	80.3	5.3
2471.924	53.6	5.6
2483.979	102.5	5.2
2484.947	88.1	5.4
2494.978	94.5	6.0
2495.941	94.7	5.8
2496.970	101.0	5.2
2505.951	65.0	6.3
2506.919	62.9	5.4
2507.851	31.3	6.1
2517.914	13.5	6.3
2519.944	−4.1	5.8
2528.862	−18.8	5.5
2529.917	−27.8	6.7
2530.887	−44.4	5.3
2531.897	−47.3	5.2
2532.858	−34.6	5.7
2541.884	−72.1	5.5
2542.825	−66.1	6.2
2543.849	−53.8	5.4
2559.876	−91.9	6.0
2560.792	−96.1	6.0
2571.766	−85.2	5.9
2573.779	−64.9	6.0
2589.758	−75.6	6.0
2590.812	−55.8	6.1
2603.749	−8.9	6.1
2604.645	−16.5	5.7
2605.685	−34.7	6.1
2615.702	43.7	5.7
2616.731	48.8	6.4
2617.620	18.7	6.6
2801.984	−2.7	5.7
2803.980	15.7	5.4
2837.959	113.0	6.9
2838.979	114.0	7.1
2839.976	71.4	5.9
2861.929	94.8	4.4
2863.972	98.8	5.3
2879.906	42.9	5.6
2881.945	0.5	9.5
2898.891	−19.1	5.2
2899.847	−50.3	5.6
2900.895	−62.0	5.2
2932.829	−75.3	5.5
2934.777	−103.2	4.7
2963.743	−81.8	5.4
2966.731	−43.3	6.0
3022.615	103.6	6.4

Table B.2. continued.

JD[a] [days]	v_{rad} [m s^{-1}]	σ_{RV} [m s^{-1}]
3232.884	24.7	4.1
3234.951	16.6	4.7
3265.858	−74.9	3.9
3268.852	−79.3	4.5
3286.776	−90.8	3.8
3355.642	55.1	5.0
3546.976	61.2	4.5
3578.894	99.0	5.6
3578.929	80.0	5.4
3578.997	55.2	5.4
3579.849	81.1	4.6
3579.946	62.1	4.3
3579.995	63.7	4.1
3580.021	65.0	4.1
3580.859	70.2	4.9
3580.939	70.4	4.5
3581.021	73.1	4.8
3581.825	74.7	4.5
3581.926	69.7	4.2
3582.022	59.2	4.4
3582.849	55.1	4.6
3582.915	54.7	4.7
3583.008	69.1	4.8
3583.931	80.6	4.2
3583.939	74.3	4.0
3583.948	74.9	4.1
3584.822	67.7	4.4
3584.870	66.0	4.2
3584.943	59.3	4.1
3585.821	38.4	3.9
3585.924	82.6	4.0
3586.010	89.9	4.3
3586.825	70.3	4.1
3586.852	64.9	4.3
3587.018	60.7	4.0
3587.921	15.6	4.2
3587.985	35.9	5.3
3698.663	−27.6	4.7
3702.650	3.4	5.5
3741.621	86.1	5.5
3911.975	107.0	4.3
3915.984	77.1	4.1
3934.930	98.3	4.3
3936.910	95.1	4.6
3967.907	−20.2	4.5
3982.797	−15.9	4.4
4054.746	−18.9	5.1
4124.594	66.1	4.4
4266.991	74.7	4.0
4297.882	134.7	4.7
4300.885	107.3	5.2
4314.872	92.0	3.9
4344.849	−19.6	4.6
4348.875	−32.3	4.7
4391.656	−35.8	6.9
4419.688	−3.5	4.8
4421.725	−4.4	5.5
4482.612	78.9	6.4
4645.956	88.1	5.3
4667.963	75.9	5.0
4711.856	−60.2	5.1
4756.777	−95.1	4.8
4777.699	−22.7	5.1

Table B.2. continued.

JD[a] [days]	v_{rad} [m s^{-1}]	σ_{RV} [m s^{-1}]
5026.951	110.8	7.3
5063.950	7.2	5.7
5097.906	−90.0	6.8
5116.818	−36.6	6.3
5155.655	60.3	8.1
5363.976	74.8	5.4
5420.911	−19.9	4.9
5449.762	−63.3	5.0
5569.617	73.5	5.1
5704.007	−4.1	4.7
5732.971	104.9	4.6
5735.972	77.3	4.8
5757.920	43.1	5.7
5803.845	−25.8	5.3
5806.857	−67.3	5.3
5829.792	−90.3	6.0
5862.718	−66.0	4.8
5894.680	27.1	7.9

Table B.3. CRIRES data for τ Gem.

JD[a] [days]	v_{rad} [m s^{-1}]	σ_{RV} [m s^{-1}]
5859.712	203	40
5918.848	324	40
5994.624	2	40
6039.424	−293	40
6244.736	252	40
6288.768	−102	40
6326.400	−317	40

Notes. [(a)] Julian date – 2 450 000.

Table B.4. CRIRES data for 91 Aqr.

JD[a] [days]	v_{rad} [m s^{-1}]	σ_{RV} [m s^{-1}]
5854.592	−116	40
6112.896	98	40
6144.640	69	40
6239.616	−11	40

Notes. [(a)] Julian date – 2 450 000.